

Modeling Membranes under a Transmembrane Potential

Lucie Delemotte, François Dehez, Werner Treptow,[†] and Mounir Tarek*

UMR Structure et Réactivité des Systèmes Moléculaires Complexes, Nancy Université, CNRS, Vandoeuvre-les-Nancy, France

Received: November 13, 2007; In Final Form: March 11, 2008

Accurate modeling of ion transport through synthetic and biological transmembrane channels has been so far a challenging problem. We introduce here a new method that allows one to study such transport under realistic biological conditions. We present results from molecular dynamics simulations of an ion channel formed by a peptide nanotube, embedded in a lipid bilayer, and subject to transmembrane potentials generated by asymmetric distributions of ions on both sides of the membrane. We show that the method is efficient for generating ionic currents and allows us to estimate the intrinsic conductance of the channel.

Introduction

The high free-energy barrier associated with the transfer of ions from the extra- to the intracellular medium rationalizes the use in cells of channels that facilitate the transport of ions across the lipid membrane. Currently, atomistic simulations remain the only techniques able to follow permeation of individual ions and solutes through transmembrane (TM) channels. Despite their potential ability to decipher key transport properties, accurate modeling of the factors that induce ionic transport has been so far challenging. In experiments, ion conduction is usually triggered by the application of a TM potential gradient (voltage) ΔV . The latter may be imposed by means of a voltage clamp or a pulse. In membrane simulations, due to the use of 3-d periodic boundary conditions (pbc), the TM voltage cannot be controlled by imposing a charge imbalance Q across the bilayer. The often used strategy is then to apply a constant electric field \vec{E} , perpendicular to the membrane plan.^{1–4} \vec{E} induces a voltage difference over the whole system $\Delta V \approx |\vec{E}| \cdot L_z$ where L_z is the size of the simulation box in the field direction. In practice, this is done by adding a force $\vec{F} = q_i \vec{E}$ to all the atoms bearing a charge q_i . Molecular dynamics (MD) simulations adopting such an approach have been used so far to study membrane electroporation^{5,6} and lipid externalization,⁷ to activate voltage-gated K channels⁸ and to determine transport properties of several ion channels.^{4,9–11}

Recently, a method allowing simulations of realistic TM potential gradients across bilayers has been proposed.¹² TM voltages are obtained using a unit cell consisting of three salt-water baths separated by two bilayers and full three-dimensional periodicity,^{13,14} inducing therefore an electric field generated by explicit ion dynamics. Here we introduce a variant of the method where consideration of the double layer is not necessary, avoiding therefore the over-cost of a large and asymmetrical system. The method considers a unique bilayer surrounded by

electrolyte baths, each terminated by an air/water interface. We present here results from all-atom MD simulations of membranes and associated ion channels, in particular peptide nanotubes, using such protocol.

First we consider a simple lipid (palmitoyl-oleyl-phosphatidylcholine, POPC) bilayer (Figure 1). Constant-pressure and constant-temperature MD simulations are performed in order to equilibrate the system at a given salt concentration using 3-d pbc. Air–water interfaces are then created at both sides of the system by extending the length of the original box. Simulations are then run at constant volume for further equilibration. Figure 2 shows the electrostatic potential (EP) (φ) maps generated from MD simulations of the bilayer in contact with water slabs each at 1 M NaCl salt concentration, considering or not a net charge imbalance Q between the electrolytes. Such a setup allows for a uniform voltage distribution above and below the lipid membrane. Note that $\varphi(z)$ is perturbed when approaching the air–water interface both due to water dipoles and to the nonuniform distribution of ions at this interface. The effect of the latter can be neglected as far as this interface is at more than 25–30 Å from the lipid. In Figure 3, we report the EP profiles $\varphi(z)$ along the normal to the membrane generated from MD simulations of the pure bilayer in contact with salt water baths (Q varying from 0 to 6e). For all simulations, $\varphi(z)$ show plateau values in the aqueous regions and an increasing potential difference between the two electrolytes indicative of a TM potential ΔV .

The linear variation of ΔV as a function of Q reported in Figure 3 shows that, as expected, the lipid bilayer behaves as a condenser. Its capacitance C , estimated considering $\Delta V = Q/C$, amounts here to 0.85 $\mu\text{F}/\text{cm}^2$. Note that capacitance values extracted from similar simulations would depend on the lipid composition (charged or not) and on the force field parameters used. Interestingly enough, in our case, it is close to the value usually assumed in the literature, e.g., 1.0 $\mu\text{F}/\text{cm}^2$.^{12,15}

It is noteworthy that, for the highest values Q imposed here, the TM voltage is large enough to induce electroporation of the membrane (data not shown). However, an appropriate choice of number of lipids, ionic concentrations, and Q can be tuned

* To whom correspondence should be addressed. Tel: (33) 3 83 68 40 95. Fax: (33) 3 83 68 43 87. E-mail: mtarek@edam.uhp-nancy.fr.

[†] Present address: Center for Molecular Modeling, Department of Chemistry, University of Pennsylvania, Philadelphia, PA 19104-6323.

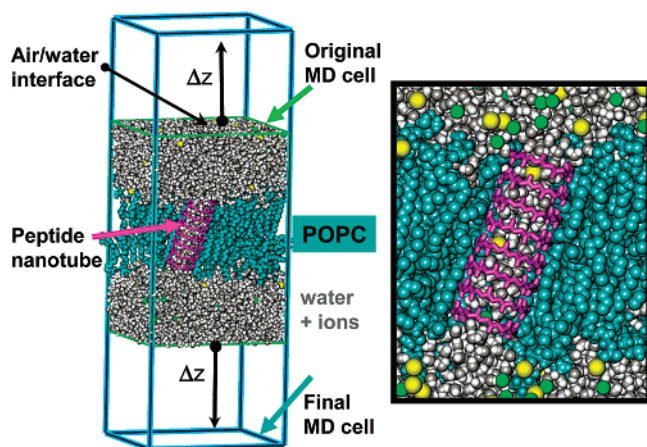


Figure 1. Left: configuration of a transmembrane peptide nanotube (purple) embedded in a hydrated POPC lipid bilayer (cyan). The cyan box represents the simulation box used to generate the 3-d periodic boundary conditions. Right: closeup view of the water (gray), Na⁺ (yellow) and Cl[−] (green) ions diffusing in the nanotube.

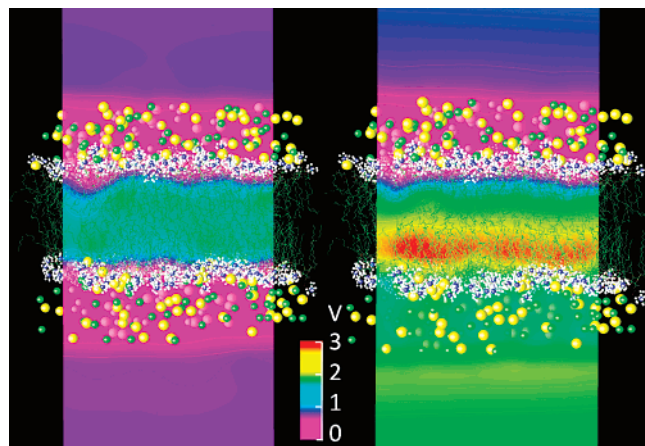


Figure 2. Electrostatic potential maps generated from the MD simulations of a POPC lipid bilayer (acyl chains, green; head groups, white) surrounded by electrolyte baths at ~ 1 M NaCl (Na⁺ yellow, Cl[−] green, water not shown) terminated by an air/water interface. Left: net charge imbalance $Q = 0e$. Right: $Q = 6e$. The 3-d potential maps are obtained by solving the Poisson equation $\nabla^2 \varphi(r) = -4\pi \sum_i \rho_i(r)$ where $\rho_i(r)$ is the point charge approximated by a spherical Gaussian, using the pmepot method.⁹

to generate TM voltages as low as 100 mV, i.e., enables working under physiological conditions. To do so, one needs to consider a larger patch of lipids, reducing therefore the net charge imbalance per unit area Q . Another possibility is to consider two dummy ions, one on each side of the membrane carrying partial charges. For the purpose of the present study, we have considered high TM voltages in order to follow ion translocation in a reasonable time scale.

In order to investigate the effect of a TM potential on transport properties of ion channels, we consider in this study a nanotube formed by the stacking of hydrophobic D-L alternated cyclic peptides, embedded in the POPC bilayer. Such peptides self-assemble into hollow tubular structures by means of a network of hydrogen bonds. Nanotubes formed for instance by peptides of 8, 10, and 12 amino acids (internal diameters ~ 7 , 10, and 13 Å^{16–19}) are shown to function as size-selective ion channels.^{17,20,21}

We have modeled the transport of ions through nanotubes formed by eight [(L-Trp-D-Leu)₆] using the present method (cf. Figure 1), assuming the same force field as in our previous investigation²² (cf. Supporting Information). The 2-d EP map

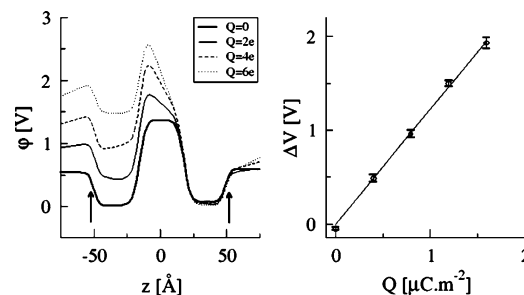


Figure 3. Left: electrostatic potential $\varphi(z)$ across a POPC lipid bilayer for different net charge imbalances Q between the upper and lower electrolytes. $\varphi(z)$ is estimated as an in-plane average of the EP distributions or may be derived directly from the MD simulations as a double integral of the charge distribution of all atoms—averaged over the membrane plans— $\rho(z)$ as, $\varphi(z) - \varphi(0) = \epsilon_0^{-1} \int \int \rho(z'') dz'' dz'$. As a reference, φ was set to zero in the upper electrolyte. The arrows indicate the position of the air–water interfaces. Right: TM potential ΔV as a function of the charge imbalance Q .

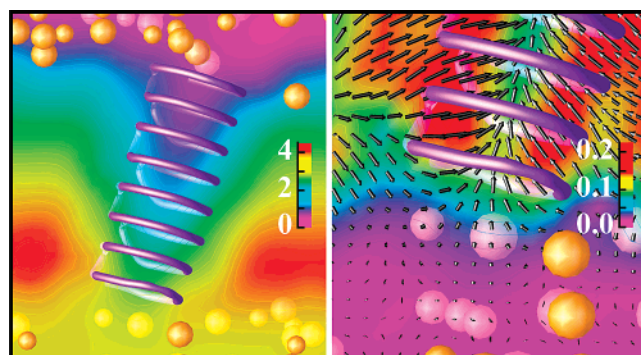


Figure 4. Left: local electrostatic potential (V) map for a TM peptide nanotube (purple) embedded in a lipid bilayer (not shown) subject to $Q = 8e$. Right: corresponding 2-d electric field maps (V/Å) derived as the gradient of the electrostatic potential. The arrows indicate the direction and strength of the field. Note that the ions appearing near the entrance of the nanotube are far behind or far in front of it.

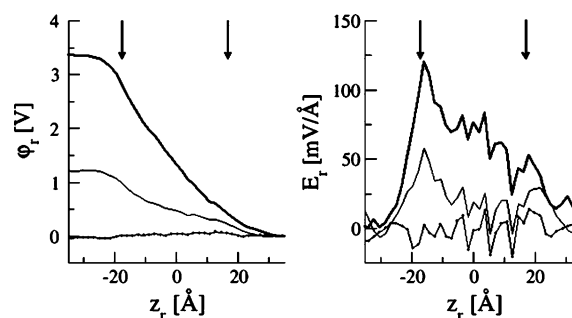


Figure 5. Left: electrostatic profile along the central axis z_r of the nanotube at different TM voltages, averaged over a radius of 2 Å around z_r . Right: corresponding electric field intensity profiles. E_r is positive when the field is oriented from the bottom to the top of the nanotube. The arrows indicate the position of the first and last rings.

of a system under $\Delta V \sim 3$ V generated by a charge imbalance $Q = 8e$ is reported in Figure 4. In contrast to the case where no TM voltage is considered,²³ the map reveals a large potential gradient, through the nanotube, giving rise to a net electric field directed along its long axis and pointing from the cathode to the anode side of the membrane. The voltage and the associated electric field profiles along the nanotube central axis z_r , generated for three different setups, are displayed in Figure 5. They clearly indicate that the voltage drop along the nanotube gives rise to a large electric field that intensity shows a maximum just at the cathode entrance of the nanotube and

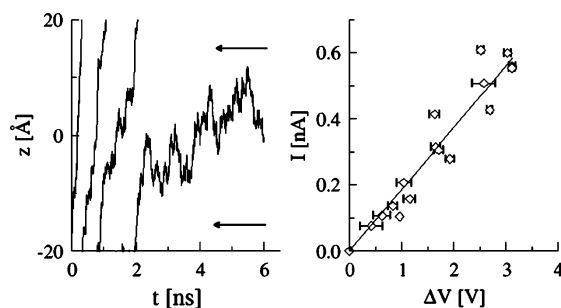


Figure 6. Left: trajectories of Na^+ ions diffusing through the nanotube as a function of time (at $t = 0$, Q is set to $8e$). The arrows delimit the location of the first and last rings. Right: intrinsic currents estimated from the ions trajectories, as a function of ΔV . Error bars are standard estimated deviations of the measured TM voltage ΔV during each full ion translocation (cf. main text).

decreases along the ionic pathway. Further analyses revealed that the voltage change at the bottom entrance of the nanotube is mainly due to water polarization. The same profiles through the bilayer (far from the nanotube) are reported in the Supporting Information and show, as expected, that the electric field is pointing toward the water slabs at both interfaces.

The electric field 2-d maps and the E_r profiles show that the electric field outside the nanotube is not null, which is indicative of an attractive funnel for cations that extends several angstroms into the water slab driving Na^+ ion translocation from the lower to the upper electrolyte. Note that the anode entrance of the channel (here set at zero voltage) presents no barrier for anionic diffusion, and we indeed notice occasionally protrusion of Cl^- ions and translocation through such wide nanotubes.

MD simulations starting from the configurations with the highest TM voltages allow one to follow Na^+ transport. After each complete translocation of an ion, the TM voltage drops due to a change ($-2e$) in the net charge imbalance. This effect is a main limitation to accurate estimates of the conductance at stationary conditions (constant voltage) that is due to size effects, making comparison of simulated ion fluxes with experimental data on channels very challenging. This can be overcome only at an extensive computational cost as the lipid patch considered in the simulation needs to be much larger.

Here, in a typical run, several ion translocations occur until ΔV reaches very low values, and then conduction is no longer favored (or too slow to be followed in the 10-ns time scale). Figure 6 shows an example of sodium ions subsequent transport events during a single MD trajectory for a system evolving from an initial condition where Q is set to $8e$. Several such simulations have been generated. For each ion translocation, we report in Figure 6 the corresponding “intrinsic current” I as a function of ΔV . The current is here calculated as $I = q/L_n(dz/dt)$, where L_z is the length of the nanotube. ΔV is the average transmembrane voltage estimated during the ion translocation in which the contribution of the ion located in the nanotube to the total TM potential has been discarded. At first approximation, ΔV can be viewed as the transmembrane potential felt by the ion. Proceeding this way, we find indeed that the estimated ΔV is almost constant during each ionic conduction. The intrinsic conductance Λ of the channel may be estimated assuming an ohmic behavior of the channel.²⁴ Λ derived from the current voltage curves (slope) amounts here to 186 pS, which is consistent with the 55 pS value measured for the narrower channel formed by [(L-Trp-D-Leu)₄].¹⁷

For comparison, we have performed several simulations using the standard “electric field” method (cf. Introduction and Supporting Information). First, we find that, for intensities

ranging from 0.04 to $0.15 \text{ V} \cdot \text{nm}^{-1}$, an electric field perpendicular to the membrane plan generates a TM voltage $\Delta V \approx |\vec{E}| \cdot L_z$ also for a system at 1 M salt concentration. Similarly, the potential maps throughout the system (both near the lipid–water interface and within the nanotube) estimated from the charge distributions are similar to those evaluated at identical ΔV with the charge imbalance method. Note, however, that for the electric field method the particles are subject to ΔV and to a constant additional force $\vec{F} = q_i \vec{E}$ that directly acts on charged particles. A total of 19 independent trajectories (total of 73 ns) were generated under electric field to estimate Na^+ intrinsic conduction within the nanotube for TM voltages ranging from 0.5 to 3 V. Using the same analysis protocol as above, we find that overall, at low to moderate ΔV , the currents are essentially identical for both methods. For high voltages, however, i.e., above 2 V, the measured Na^+ ionic currents were sensibly higher for the electric field method (cf. Supporting Information). This is an expected result as the applied force $\vec{F} = q_i \vec{E}$ becomes significant at high-intensity electric fields. The effect of such additional force turned out to be large enough to favor conduction of Cl^- ions (during a total of 22 ns runs, 10 complete Cl^- passages were witnessed over 24 Na^+ passages). In conclusion, for the present system, we do not find a significant difference between this approach and the electric field method for ionic conduction at low to moderate TM voltages. The latter method, however, presents the disadvantage of intrinsically considering an additional force component that may influence charge distribution and dipoles reorientation in complex environments such as inside a protein. Further specific studies are required to shed light onto this. Note that this component may be reduced if one considers a system large enough ($|\vec{E}| \approx \Delta V/L_z$).

In summary, the results presented here concern a simple nanotube, for which the ionic transport properties have been derived from unconstrained MD simulations. For computational efficiency, high transmembrane voltages (500 mV–3 V) were applied. While these are large enough to induce membrane electroporation, interestingly enough, charge imbalance adjustment due to ionic transport is fast enough to release the stress on the membrane avoiding disruption of its integrity. Several electrostatic properties of the channel have been investigated and could potentially be confronted to models based on continuum approaches.^{25–27} The method presented here can easily be implemented to study more complex ion channels for which fine-tuned interactions and specific molecular rearrangement are required for ionic transport (an example of a bacterial potassium channel is given in the Supporting Information).

The approach considering charge imbalances is very suitable for the study of ionic transport through TM channels or the investigation of the effect of TM potentials on peptides and membrane proteins. It further allows investigation of other important aspects such as the effect of asymmetric salt concentrations (chemical potential gradients) on transport properties. We anticipate therefore that this method will find a broad range of applications in modeling realistic biological systems.

Acknowledgment. The authors are grateful to Olivier Collet for insightful discussions. Calculations were partly performed at the Centre Informatique National de l’Enseignement Supérieur (Cines) Montpellier, France.

Supporting Information Available: Materials and methods. Electrostatic potential and electric field 1-d profiles across the membrane for the system at several TM voltages. Movies of Na^+ ion translocation through the peptide channel. Movie of K^+ translocation through MthK, a bacterial potassium channel

using the method introduced here. This material is available free of charge via the Internet at <http://pubs.acs.org>.

References and Notes

- (1) Suenaga, A.; Komeiji, Y.; Uebayasi, M.; Meguro, T.; Saito, M.; Yamato, I. *Biosci. Rep.* **1998**, *18*, 39.
- (2) Zhong, Q.; Moore, P. B.; Newns, D. M.; Klein, M. L. *FEBS Lett.* **1998**, *427*, 267.
- (3) Tieleman, D. P.; Berendsen, J. H. C.; Sansom, M. S. P. *Biophys. J.* **2001**, *80*, 331.
- (4) Crozier, P. S.; Henderson, D.; Rowley, R. L.; Busath, D. D. *Biophys. J.* **2001**, 3077.
- (5) Anézo, C.; de Vries, A. H.; Hölte, H. D.; Tieleman, D. P.; Marrink, S. J. *J. Phys. Chem. B* **2003**, *107*, 9424.
- (6) Tarek, M. *Biophys. J.* **2005**, *88*, 4045.
- (7) Vernier, P. T.; Ziegler, M. J.; Sun, Y.; Chang, W. V.; Gundersen, M. A.; Tieleman, D. P. *J. Am. Chem. Soc.* **2006**, *128*, 6288.
- (8) Treptow, W.; Maigret, B.; Chipot, C.; Tarek, M. *Biophys. J.* **2004**, *87*, 2365.
- (9) Aksimentiev, A.; Schulten, K. *Biophys. J.* **2005**, *88*, 3745.
- (10) Park, S.; Khalili-Araghi, F.; Tajkhorshid, E.; Schulten, K. *J. Chem. Phys.* **2003**, *119*, 3559.
- (11) Sotomayor, M.; Schulten, K. *Biophys. J.* **2004**, *87*, 3050.
- (12) Sachs, J. N.; Crozier, P. S.; Woolf, T. B. *J. Chem. Phys.* **2004**, *121*, 10847.
- (13) Gurtovenko, A. A.; Vattulainen, I. *J. Am. Chem. Soc.* **2005**, *127*, 17570.
- (14) Kandasamy, S. K.; Larson, R. G. *J. Chem. Phys.* **2006**, *125*, 074901.
- (15) Roux, B. *Biophys. J.* **1997**, *73*, 2980.
- (16) Ghadiri, M. R.; Granja, J. R.; Milligan, R. A.; McRee, D. E.; Khazanovich, N. *Nature* **1993**, *366*, 324.
- (17) Ghadiri, M. R.; Granja, J. R.; Buehler, L. *Nature* **1994**, *369*, 301.
- (18) Granja, J. R.; Ghadiri, M. R. *J. Am. Chem. Soc.* **1994**, *116*, 10785.
- (19) Khazanovich, N.; Granja, J. R.; McRee, D. E.; Milligan, R. A.; Ghadiri, M. R. *J. Am. Chem. Soc.* **1994**, *116*, 6011.
- (20) Motesharei, K.; Ghadiri, M. R. *J. Am. Chem. Soc.* **1997**, *119*, 11306.
- (21) Asthagiri, D.; Bashford, D. *Biophys. J.* **2002**, *82*, 1176.
- (22) Tarek, M.; Maigret, B.; Chipot, C. *Biophys. J.* **2003**, *85*, 2287–2298.
- (23) Dehez, F.; Tarek, M.; Chipot, C. *J. Phys. Chem. B* **2007**, *111*, 10633.
- (24) Sanchez-Quesada, J.; Isler, M. P.; Ghadiri, M. R. *J. Am. Chem. Soc.* **2002**, *124*, 10004.
- (25) Mamonov, A. B.; Coalson, R. D.; Nitzan, A.; Kurnikova, M. G. *Biophys. J.* **2003**, *84*, 3646.
- (26) Prosser, R. S.; Hwang, J. S.; Vold, R. R. *Biophys. J.* **1998**, *74*, 2405.
- (27) Saranati, M.; Aboud, S.; Eisenberg, R. *Rev. Comp. Chem.* **2006**, *22*, 229.